Supplement of Atmos. Chem. Phys., 23, 611–636, 2023
https://doi.org/10.5194/acp-23-611-2023-supplement

Atmospheric Chemistry and Physics
Open Access

*Supplement of*

# Impact of aging on the sources, volatility, and viscosity of organic aerosols in Chinese outflows

**Tingting Feng et al.**

*Correspondence to:* Weiwei Hu (weiweihu@gig.ac.cn)

## 1.1 PMF and ME-2 analysis

The initial high-resolution OA data and error matrix ranging from m/z 12 to m/z 120 were put into the PMF analysis of this study, while the isotope ions and ions with the low signal-to-noise ratio (SNR < 0.2) were removed. Ions with weak SNR (0.2 < SNR < 2) and $CO_2^+$ related ions ($CO_2^+$, $CO^+$, $H_2O^+$, $HO^+$, $O^+$) were downweighed by increasing the error with a factor of 2.23 (Zhang et al., 2011; Ulbrich et al., 2009).

At first, unconstrained source apportionment was conducted (seed=0) using PMF Evaluation Tool (PET, version 2.08) (Ulbrich et al., 2009). As the $Q/Q_{exp}$ decreases (Fig. S3), no biomass burning factor was resolved in 3-4 factor solutions (Figs. S4 and S5). However, biomass burning was indeed seen during the campaign. Biomass burning-related factor was resolved when 5-7 factors were chosen, while they are not applicable due to splitting OOA factors (for example 5-factor solution in Fig. S6). Thus, the ME-2 method was applied here. As mentioned in the PMF results, it can be found that 4-5 factors are better solutions, because fewer factors cannot resolve the BBOA factor, whereas more factors will result in meaningless OOA factors. Then, we constrained HOA (from Beijing) and BBOA (from Changdao) in ambient and ambient + TD datasets using SoFi v6.81 with different α values from 0 to 1, where α value represents the constrained extent in the standard mass spectral profile (Zhang et al., 2011; Huang et al., 2014; Canonaco et al., 2013). To ensure the results of source apportionment, OA factors from ambient and ambient + TD datasets should show similar variations. However, time series from ambient and ambient + TD are different when 4 factors with α value of 0 were chosen (Fig. S7), thus 4 factors with HOA and BBOA being constrained in ME-2 here is not the best solution. When 5 factors were chosen, a splitting of the HOA time series was found (Fig. S8). The constrained HOA shows very low contributions to total OA (< 4 %) and is noisy, especially during the TD sampling. Such noisy time series will lead to a large uncertainty when calculating MFR (mass fraction remaining). Meanwhile, the constrained HOA factor exhibits a very similar variation to the aged-HOA here (Fig. S9, R=0.52). Thus, we do not think the 5-factor solution with both HOA and BBOA being constrained is good as well. Instead, we only constrain BBOA without HOA, since the aged-HOA can be resolved in PMF. Here, strong BBOA obtained from the Changdao campaign, which was conducted in a similar season and nearby location to Dongying (Hu et al., 2013), was chosen. A difference exists in the OOA2 factor between the time series of ambient and ambient + TD in the 5-factor solution (Fig. S10). Therefore, 4 factors with BBOA being constrained (a value=0) is the most environmentally meaningful solution. As shown in Fig. S11, there is a good correlation between the ambient and ambient + TD datasets, which can be used to investigate the volatilities of different OA factors. In this solution, the BBOA factor was resolved by constraining the BBOA spectrum from the Changdao campaign. The other POA is considered to be aged-HOA rather than COA/CCOA for the following reasons: (1) First of all, we do not identify the PAH ions with high abundance in this mass spectrum like CCOA in the spring of Changdao (Fig. S12(c)), so CCOA is not the priority we considered here. (2) The ratio between $f_{55}$ versus $f_{57}$ is different in HOA (0.9-1.1) and COA (2.2-2.8) spectra, which is driven by the oxygen-containing ions, $C_3H_3O^+$ and $C_3H_5O^+$(Mohr et al., 2012). In this study, the scatterplots of $f_{55}$ versus $f_{57}$, which subtracted the interferences of OOA, are closer to the COA source in the urban areas than HOA sources (Fig. S12(d)). However, the higher $f_{55}/f_{57}$ value in ambient OA is not driven by the aged-HOA. E.g., as the fraction of aged-HOA in total OA goes up, the $f_{55}$ vs $f_{57}$ ratios do not change (Fig. S12(d)). The value of $f_{55}$ versus $f_{57}$ of aged-HOA is 1.8, which is also similar to that of BBOA and lower than those of the other two OOA factors (Fig. S12(d)). Thus, the higher value of $f_{55}$ vs $f_{57}$ here is probably due to the oxidation of HOA during transportation. To further investigate if the cooking impact the OA in this study, another cooking tracer $f_{98}$ was investigated here. We compared the scatterplots between $f_{44}$ vs. $f_{98}$ with other field campaigns that were impacted by the cooking or not. As shown in Fig. S13. no enhancement of $f_{98}$ was found in this study compared to other studies, suggesting the cooking did not show an obvious impact on OA observed in this site. In addition, the two peaks in the dining time were not found in the aged-HOA factor. The evidence to support the aged-HOA is from vehicle emissions based on the relationship between some traffic tracers and aged-HOA. As mentioned in Fig. S14, factor 2 (that is aged-HOA) is highly correlated with typical traffic tracers, such as BC, $NO_2$, and benzene (R>0.6). Therefore, the other POA factor is considered as HOA originated from vehicle emissions in this study. In addition, when the standard HOA spectrum was constrained, the time series of that POA is similar to the trend of aged-HOA (Fig. S15), which confirmed the existence of aged-HOA factor.

## 1.2 Calibrations of transmission and temperature of TD

We used the formula proposed by Huffman et al. (2008) to calibrate the transmission and temperature of TD since their residence times are similar (about 21s).

$$\text{TD Transmission} = -0.00082 * \text{Temp}_{\text{centerline, real}} + 0.98 \qquad (1)$$

Where TD transmission represents the aerosol mass ratio between TD and ambient lines due to particle loss. Temp $_{\text{centerline, real}}$ is the real centerline temperature, which was found to be about 17 % higher than the set temperature controlled by TD software (Temp $_{\text{TD-set}}$). The centerline temperature can be corrected with the following eq. (2):

$$\text{Temp}_{\text{centerline, real}} = 1.1732 * \text{Temp}_{\text{TD-set}} - 7.7625 \qquad (2)$$

To compare the thermograms from different experiments with the similar TD setup, each mass thermogram was fitted by the Hill's Equation, a type of sigmoidal function, to obtain the $T_{50}$ value, which is the temperature at which MFR = 0.50 (Kolesar et al., 2015; Emanuelsson et al., 2013).

$$MFR(T) = MFR_{max} + \left(\frac{MFR_{min} - MFR_{max}}{1+(\frac{T_{50}}{T})^{S_{MFR}}}\right) \qquad (3)$$

where $MFR_{min}$ and $MFR_{max}$ are the MFR values at the highest and lowest temperatures, $S_{MFR}$ is the slope representing the steepness of the curve of MFR.

### 1.3 Predictions of glass transition temperature and viscosity of organic aerosols

The glass transition temperature ($T_g$) represents the temperature where phase transition occurs between semisolid and glassy states. $T_g$ of organic aerosols can be estimated based on the volatility distributions, as shown in Eq. (4):

$$T_{g,i} = 289.10 - 16.5 \times \log_{10}(C_i{}^0) - 0.29 \times [\log_{10}(C_i{}^0)]^2 + 3.23 \times \log_{10}(C_i{}^0) \times (O:C) \tag{4}$$

where $C_i^0$ is saturation vapor pressure ($C^*$, unit: μg $m^{-3}$) at 298 K and O:C is determined by the A-A method (Unit: dimensionless). Then the $T_g$ of organic aerosols ($T_{g,org}$) under dry conditions can be calculated by a simplified Gordon–Taylor equation assuming the Gordon–Taylor constant ($k_{GT}$) =1 as shown in Eq. (5), where $\omega_i$ is the fraction of particulate organic aerosols per volatility bin (Dette et al., 2014).

$$T_{g,org} = \sum_i \omega_i T_{g,i} \tag{5}$$

In addition, Gordon–Taylor equation is also used to calculate $T_g$ of organic-water ($T_{g,\omega org}$) mixture at a given RH by assuming $k_{GT}$=2.5.

$$T_{g,\omega_{org}} = \frac{(1-\omega_{org})T_{g,w} + \frac{1}{k_{GT}}\omega_{org}T_{g,org}}{(1-\omega_{org}) + \frac{1}{k_{GT}}\omega_{org}} \tag{6}$$

$T_{g,w}$ represents the glass transition temperature of the water, generally 136 K (Koop et al., 2011). $\omega_{org}$ ($\omega_{org}$=$m_{OA}$/$m_{OA}$+$m_{H2O}$) is the mass fraction of organic species ($m_{OA}$) and water ($m_{H2O}$) in the particle phase. The total mass concentration of water can be determined by effective hygroscopicity parameters of organics $\kappa_{org}$ ( $\kappa_{org}$= 2.10 (± 0.07) × $f_{44}$ − 0.11 (± 0.01) ), where $f_{44}$ is the fraction of m/z 44 signal in total organic signals (Mei et al., 2013).

$$m_{H2O} = \frac{\kappa_{org}\rho_w m_{org}}{\rho_{org}(\frac{1}{a_w}-1)} \tag{7}$$

The density of organic aerosols ($\rho_{org}$) and the water ($\rho_w$) in this study were estimated to be 1.44 g $cm^{-3}$ (Kuwata et al., 2012) and 1g $cm^{-3}$, respectively. $a_w$ represents water activity, which is calculated by $a_w$ = RH/100.

Then we can calculate temperature-dependent viscosity (η) by the modified Vogel-Tammann-Fulcher (VTF) equation (Eq. (8)).

$$\eta = \eta_{\infty} e^{\frac{T_0 D}{T - T_0}}$$

(8) where $\eta_{\infty}$ $=10^{-5}$ Pa s, $T_0 = \frac{39.17\, T_{g,\omega org}}{D+39.17}$. D is the fragility parameter usually assumed to be 10 (DeRieux et al., 2018).

The timescale of particle diffusion is characterized by mixing time ($\tau_{mix}$) according to Eq. (9), where $d_p$ is the particle diameter ($d_p$ of ambient OA is about 550 nm, which is assumed 200 nm here for comparison with other studies conveniently (Xu et al., 2021; Li et al., 2020; Evoy et al., 2019)), and the bulk diffusion coefficient $D_b$ is calculated from the predicted viscosity by the fractional Stokes-Einstein relation, as shown in Eq. (10) (Xu et al., 2021; Evoy et al., 2019; Li et al., 2020).

$$\tau_{\mathrm{mix}} = \frac{d_p^2}{4\pi^2 D_b} \tag{9}$$

$$D_b = D_c(\frac{\eta_c}{\eta})^{\xi} \tag{10}$$

in which $\xi$ is an empirical fit parameter and we used 0.93 here, $\eta_c$ is the crossover viscosity and we used $10^{-3}$ Pa s here. $D_c$ is the crossover diffusion coefficient where the fractional Stokes-Einstein (Eq. (10)) and the Stokes-Einstein (Eq. (11)) predict the same diffusion coefficient (Evoy et al., 2019). In the Stokes-Einstein equation, k, and $R_H$ are Boltzmann constant and diffusing radius respectively, T and $\eta$ represent temperature and viscosity in ambient air.

$$D_c = \frac{kT}{6\pi\eta R_H} \tag{11}$$

## 1.4 Inorganic nitrate and organic nitrate

During the calibration, the measured $NO_x$ ratio ($NO_2^+/NO^+$) of standard ammonium nitrate particles ($R_{NH4NO3}$) was determined to be 0.28 (Fig. S16a). The $NO_2^+/NO^+$ ratio of organic nitrate ($R_{ONO2}$) was estimated by dividing $R_{NH4NO3}$ by a factor of 2.75 proposed by Day et al. (2022), thus the $R_{ONO2}$ ratio in this study is 0.1. The fraction of organic nitrate and inorganic nitrate can be estimated based on the following equations (Farmer et al., 2010):

$$f_{\mathrm{RONO2}} = \frac{(R_{amb} - R_{\mathrm{NH4NO3}})(1 + R_{\mathrm{ONO2}})}{(R_{\mathrm{ONO2}} - R_{\mathrm{NH4NO3}})(1 + R_{amb})} \tag{12}$$

$$f_{\mathrm{RONO2}} = 1 \ \ (f_{\mathrm{RONO2}} > 1) \tag{13}$$

$$f_{\mathrm{NH4NO3}} = 1 - f_{\mathrm{RONO2}} \ \ (0 < f_{\mathrm{RONO2}} < 1) \tag{14}$$

$$f_{\mathrm{NH4NO3}} = 1 \ (f_{\mathrm{RONO2}} < 0) \tag{15}$$

**References:**

Canonaco, F., Crippa, M., Slowik, J. G., Baltensperger, U., and Prévôt, A. S. H.: SoFi, an IGOR-based interface for the efficient use of the generalized multilinear engine (ME-2) for the source apportionment: ME-2 application to aerosol mass spectrometer data, Atmospheric Measurement Techniques, 6, 3649-3661, 10.5194/amt-6-3649-2013, 2013.

Cappa, C. D. and Jimenez, J. L.: Quantitative estimates of the volatility of ambient organic aerosol, Atmospheric Chemistry and Physics, 10, 5409-5424, 10.5194/acp-10-5409-2010, 2010.

Cubison, M. J., Ortega, A. M., Hayes, P. L., Farmer, D. K., Day, D., Lechner, M. J., Brune, W. H., Apel, E., Diskin, G. S., Fisher, J. A., Fuelberg, H. E., Hecobian, A., Knapp, D. J., Mikoviny, T., Riemer, D., Sachse, G. W., Sessions, W., Weber, R. J., Weinheimer, A. J., Wisthaler, A., and Jimenez, J. L.: Effects of aging on organic aerosol from open biomass burning smoke in aircraft and laboratory studies, Atmospheric Chemistry and Physics, 11, 12049-12064, 10.5194/acp-11-12049-2011, 2011.

Day, D. A., Campuzano-Jost, P., Nault, B. A., Palm, B. B., Hu, W., Guo, H., Wooldridge, P. J., Cohen, R. C., Docherty, K. S., Huffman, J. A., de Sá, S. S., Martin, S. T., and Jimenez, J. L.: A Systematic Re-evaluation of Methods for Quantification of Bulk Particle-phase Organic Nitrates Using Real-time Aerosol Mass Spectrometry, Atmos. Meas. Tech. Discuss., 2021, 1-35, 10.5194/amt-2021-263, 2021.

Day, D. A., Campuzano-Jost, P., Nault, B. A., Palm, B. B., Hu, W., Guo, H., Wooldridge, P. J., Cohen, R. C., Docherty, K. S., Huffman, J. A., de Sá, S. S., Martin, S. T., and Jimenez, J. L.: A systematic re-evaluation of methods for quantification of bulk particle-phase organic nitrates using real-time aerosol mass spectrometry, Atmospheric Measurement Techniques, 15, 459-483, 10.5194/amt-15-459-2022, 2022.

DeRieux, W. S., Li, Y., Lin, P., Laskin, J., Laskin, A., Bertram, A. K., Nizkorodov, S. A., and Shiraiwa, M.: Predicting the glass transition temperature and viscosity of secondary organic material using molecular composition, Atmospheric Chemistry and Physics, 18, 6331-6351, 10.5194/acp-18-6331-2018, 2018.

Dette, H. P., Qi, M., Schroder, D. C., Godt, A., and Koop, T.: Glass-forming properties of 3-methylbutane-1,2,3-tricarboxylic acid and its mixtures with water and pinonic acid, J Phys Chem A, 118, 7024-7033, 10.1021/jp505910w, 2014.

Emanuelsson, E. U., Watne, A. K., Lutz, A., Ljungstrom, E., and Hallquist, M.: Influence of humidity, temperature, and radicals on the formation and thermal properties of secondary organic aerosol (SOA) from ozonolysis of beta-pinene, J Phys Chem A, 117, 10346-10358, 10.1021/jp4010218, 2013.

Evoy, E., Maclean, A. M., Rovelli, G., Li, Y., Tsimpidi, A. P., Karydis, V. A., Kamal, S., Lelieveld, J., Shiraiwa, M., Reid, J. P., and Bertram, A. K.: Predictions of diffusion rates of large organic molecules in secondary organic aerosols using the Stokes–Einstein and fractional Stokes–Einstein relations, Atmospheric Chemistry and Physics, 19, 10073-10085, 10.5194/acp-19-10073-2019, 2019.

Farmer, D. K., Matsunaga, A., Docherty, K. S., Surratt, J. D., Seinfeld, J. H., Ziemann, P. J., and Jimenez, J. L.: Response of an aerosol mass spectrometer to organonitrates and organosulfates and implications for atmospheric chemistry, Proc Natl Acad Sci U S A, 107, 6670-6675, 10.1073/pnas.0912340107, 2010.

Faulhaber, A. E., Thomas, B. M., Jimenez, J. L., Jayne, J. T., Worsnop, D. R., and Ziemann, P. J.: Characterization of a thermodenuder-particle beam mass spectrometer system for the study of organic aerosol volatility and composition, Atmos. Meas. Tech., 2009.

Grieshop, A. P., Logue, J. M., Donahue, N. M., and Robinson, A. L.: Laboratory investigation of photochemical oxidation of organic aerosol from wood fires 1: measurement and simulation of organic aerosol evolution, Atmos. Chem. Phys., 9, 1263-1277, 10.5194/acp-9-1263-2009, 2009a.

Grieshop, A. P., Miracolo, M. A., Donahue, N. M., and Robinson, A. L.: Constraining the Volatility Distribution and Gas-Particle Partitioning of Combustion Aerosols Using Isothermal Dilution and Thermodenuder Measurements, Environmental Science & Technology, 43, 4750-4756, 10.1021/es8032378, 2009b.

Hu, W., Hu, M., Hu, W., Jimenez, J. L., Yuan, B., Chen, W., Wang, M., Wu, Y., Chen, C., Wang, Z., Peng, J., Zeng, L., and Shao, M.: Chemical composition, sources, and aging process of submicron aerosols in Beijing: Contrast between summer and winter, Journal of Geophysical Research: Atmospheres, 121, 1955-1977, 10.1002/2015jd024020, 2016a.

Hu, W., Palm, B. B., Day, D. A., Campuzano-Jost, P., Krechmer, J. E., Peng, Z., de Sá, S. S., Martin, S. T., Alexander, M. L., Baumann, K., Hacker, L., Kiendler-Scharr, A., Koss, A. R., de Gouw, J. A., Goldstein, A. H., Seco, R., Sjostedt, S. J., Park, J.-H., Guenther, A. B., Kim, S., Canonaco, F., Prévôt, A. S. H., Brune, W. H., and Jimenez, J. L.: Volatility and lifetime against OH heterogeneous reaction of ambient
isoprene-epoxydiols-derived secondary organic aerosol (IEPOX-SOA), Atmospheric Chemistry and Physics, 16, 11563-11580, 10.5194/acp-16-11563-2016, 2016b.

Hu, W. W., Hu, M., Yuan, B., Jimenez, J. L., Tang, Q., Peng, J. F., Hu, W., Shao, M., Wang, M., Zeng, L. M., Wu, Y. S., Gong, Z. H., Huang, X. F., and He, L. Y.: Insights on organic aerosol aging and the influence of coal combustion at a regional receptor site of central eastern China, Atmospheric Chemistry and Physics, 13, 10095-10112, 10.5194/acp-13-10095-2013, 2013.

Huang, R. J., Zhang, Y., Bozzetti, C., Ho, K. F., Cao, J. J., Han, Y., Daellenbach, K. R., Slowik, J. G., Platt, S. M., Canonaco, F., Zotter, P., Wolf, R., Pieber, S. M., Bruns, E. A., Crippa, M., Ciarelli, G., Piazzalunga, A., Schwikowski, M., Abbaszade, G., Schnelle-Kreis, J., Zimmermann, R., An, Z., Szidat, S., Baltensperger, U., El Haddad, I., and Prevot, A. S.: High secondary aerosol contribution to particulate pollution during haze events in China, Nature, 514, 218-222, 10.1038/nature13774, 2014.

Huffman, J. A., Ziemann, P. J., Jayne, J. T., Worsnop, D. R., and Jimenez, J. L.: Development and Characterization of a Fast-Stepping/Scanning Thermodenuder for Chemically-Resolved Aerosol Volatility Measurements, Aerosol Science and Technology, 42, 395-407, 10.1080/02786820802104981, 2008.

Kolesar, K. R., Chen, C., Johnson, D., and Cappa, C. D.: The influences of mass loading and rapid dilution of secondary organic aerosol on particle volatility, Atmospheric Chemistry and Physics, 15, 9327-9343, 10.5194/acp-15-9327-2015, 2015.

Koop, T., Bookhold, J., Shiraiwa, M., and Pöschl, U.: Glass transition and phase state of organic compounds: dependency on molecular properties and implications for secondary organic aerosols in the atmosphere, Physical Chemistry Chemical Physics, 13, 19238-19255, 10.1039/C1CP22617G, 2011.

Kuwata, M., Zorn, S. R., and Martin, S. T.: Using elemental ratios to predict the density of organic material composed of carbon, hydrogen, and oxygen, Environ Sci Technol, 46, 787-794, 10.1021/es202525q, 2012.

Li, X., Dallmann, T. R., May, A. A., Tkacik, D. S., Lambe, A. T., Jayne, J. T., Croteau, P. L., and Presto, A. A.: Gas-Particle Partitioning of Vehicle Emitted Primary Organic Aerosol Measured in a Traffic Tunnel, Environ Sci Technol, 50, 12146-12155, 10.1021/acs.est.6b01666, 2016.

Li, Y., Day, D. A., Stark, H., Jimenez, J. L., and Shiraiwa, M.: Predictions of the glass transition temperature and viscosity of organic aerosols from volatility distributions, Atmospheric Chemistry and Physics, 20, 8103-8122, 10.5194/acp-20-8103-2020, 2020.

Louvaris, E. E., Florou, K., Karnezi, E., Papanastasiou, D. K., Gkatzelis, G. I., and Pandis, S. N.: Volatility of source apportioned wintertime organic aerosol in the city of Athens, Atmospheric Environment, 158, 138-147, 10.1016/j.atmosenv.2017.03.042, 2017.

May, A. A., Presto, A. A., Hennigan, C. J., Nguyen, N. T., Gordon, T. D., and Robinson, A. L.: Gas-particle partitioning of primary organic aerosol emissions: (2) diesel vehicles, Environ Sci Technol, 47, 8288-8296, 10.1021/es400782j, 2013a.

May, A. A., Presto, A. A., Hennigan, C. J., Nguyen, N. T., Gordon, T. D., and Robinson, A. L.: Gas-particle partitioning of primary organic aerosol emissions: (1) Gasoline vehicle exhaust, Atmospheric Environment, 77, 128-139, 10.1016/j.atmosenv.2013.04.060, 2013b.

May, A. A., Levin, E. J. T., Hennigan, C. J., Riipinen, I., Lee, T., Collett, J. L., Jimenez, J. L., Kreidenweis, S. M., and Robinson, A. L.: Gas-particle partitioning of primary organic aerosol emissions: 3. Biomass burning, Journal of Geophysical Research: Atmospheres, 118, 11,327-311,338, 10.1002/jgrd.50828, 2013c.

Mei, F., Setyan, A., Zhang, Q., and Wang, J.: CCN activity of organic aerosols observed downwind of urban emissions during CARES, Atmospheric Chemistry and Physics, 13, 12155-12169, 10.5194/acp-13-12155-2013, 2013.

Mohr, C., DeCarlo, P. F., Heringa, M. F., Chirico, R., Slowik, J. G., Richter, R., Reche, C., Alastuey, A., Querol, X., Seco, R., Peñuelas, J., Jiménez, J. L., Crippa, M., Zimmermann, R., Baltensperger, U., and Prévôt, A. S. H.: Identification and quantification of organic aerosol from cooking and other sources in Barcelona using aerosol mass spectrometer data, Atmospheric Chemistry and Physics, 12, 1649-1665, 10.5194/acp-12-1649-2012, 2012.

Ng, N. L., Canagaratna, M. R., Zhang, Q., Jimenez, J. L., Tian, J., Ulbrich, I. M., Kroll, J. H., Docherty, K. S., Chhabra, P. S., Bahreini, R., Murphy, S. M., Seinfeld, J. H., Hildebrandt, L., Donahue, N. M., DeCarlo, P. F., Lanz, V. A., Prévôt, A. S. H., Dinar, E., Rudich, Y., and Worsnop, D. R.: Organic aerosol components observed in Northern Hemispheric datasets from Aerosol Mass Spectrometry, Atmospheric Chemistry and Physics, 10, 4625-4641, 10.5194/acp-10-4625-2010, 2010.

Paciga, A., Karnezi, E., Kostenidou, E., Hildebrandt, L., Psichoudaki, M., Engelhart, G. J., Lee, B.-H., Crippa, M., Prévôt, A. S. H., Baltensperger, U., and Pandis, S. N.: Volatility of organic aerosol and its components in the megacity of Paris, Atmospheric Chemistry and Physics, 16, 2013-2023, 10.5194/acp-16-2013-2016, 2016.

Sato, K., Fujitani, Y., Inomata, S., Morino, Y., Tanabe, K., Hikida, T., Shimono, A., Takami, A., Fushimi, A., Kondo, Y., Imamura, T., Tanimoto, H., and Sugata, S.: A study of volatility by composition, heating, and dilution measurements of secondary organic aerosol from 1,3,5-trimethylbenzene, Atmospheric Chemistry and Physics, 19, 14901-14915, 10.5194/acp-19-14901-2019, 2019.

Sato, K., Fujitani, Y., Inomata, S., Morino, Y., Tanabe, K., Ramasamy, S., Hikida, T., Shimono, A., Takami, A., Fushimi, A., Kondo, Y., Imamura, T., Tanimoto, H., and Sugata, S.: Studying volatility from composition, dilution, and heating measurements of secondary organic aerosols formed during α-pinene ozonolysis, Atmospheric Chemistry and Physics, 18, 5455-5466, 10.5194/acp-18-5455-2018, 2018.

Ulbrich, I. M., Canagaratna, M. R., Zhang, Q., Worsnop, D. R., and Jimenez, J. L.: Interpretation of organic components from Positive Matrix Factorization of aerosol mass spectrometric data, Atmos. Chem. Phys., 9, 2891-2918, 10.5194/acp-9-2891-2009, 2009.

Xu, W., Chen, C., Qiu, Y., Li, Y., Zhang, Z., Karnezi, E., Pandis, S. N., Xie, C., Li, Z., Sun, J., Ma, N., Xu, W., Fu, P., Wang, Z., Zhu, J., Worsnop, D. R., Ng, N. L., and Sun, Y.: Organic aerosol volatility and viscosity in the North China Plain: contrast between summer and winter, Atmospheric Chemistry and Physics, 21, 5463-5476, 10.5194/acp-21-5463-2021, 2021.

Ylisirniö, A., Buchholz, A., Mohr, C., Li, Z., Barreira, L., Lambe, A., Faiola, C., Kari, E., Yli-Juuti, T., Nizkorodov, S. A., Worsnop, D. R., Virtanen, A., and Schobesberger, S.: Composition and volatility of secondary organic aerosol (SOA) formed from oxidation of real tree emissions compared to simplified volatile organic compound (VOC) systems, Atmospheric Chemistry and Physics, 20, 5629-5644, 10.5194/acp-20-5629-2020, 2020.

Zhang, Q., Jimenez, J. L., Canagaratna, M. R., Ulbrich, I. M., Ng, N. L., Worsnop, D. R., and Sun, Y.: Understanding atmospheric organic aerosols via factor analysis of aerosol mass spectrometry: a review, Analytical and Bioanalytical Chemistry, 401, 3045-3067, 10.1007/s00216-011-5355-y, 2011.

**Table S1. Introduction on instruments for VOCs, criteria regular gases and black carbon (BC)**

| Species | Instruments | Mode | Time resolution |
|---|---|---|---|
| **Volatile organic compounds (VOCs)** | on-line GC-FID | | 1 hour |
| **NOx** | Chemiluminescence NO-$NO_2$-$NO_x$ Analyzer | Thermo 42i | 1 min |
| **$SO_2$** | Pulsed Fluorescence $SO_2$ Analyzer | Thermo 43i | 1 min |
| **CO** | Trace Level Enhanced CO Analyzer | Thermo 48i | 1 min |
| **$O_3$** | Ozone Monitor | Thermo 49i | 1 min |
| **BC** | 7-band Aethalometer | Magee AE31 | 5 min |

**Table S2. Summary of fractions of ELVOCs, LVOCs and S/IVOCs of OA, the residence time (RT) of TD as well as the O:C of aerosols.**

| Anthropogenic | ELVOCs | LVOCs | S/IVOCs | O:C | RT(s) | References |
|---|---|---|---|---|---|---|
| Beijing (winter) | 0.12 | 0.21 | 0.67 | 0.34 | 10 | (Xu et al., 2021) |
| Gucheng (winter) | 0.1 | 0.25 | 0.65 | 0.4 | 10 | (Xu et al., 2021) |
| Beijing (summer) | 0.13 | 0.235 | 0.635 | 0.53 | 7.4 | (Xu et al., 2021) |
| Mexico City (spring) | 0.27 | 0.31 | 0.42 | 0.52 | 21.2 | (Cappa and Jimenez, 2010) |
| Athens (winter) | 0.3 | 0.33 | 0.37 | 0.32 | 28 | (Louvaris et al., 2017) |
| Paris (summer) | 0.25 | 0.38 | 0.37 | 0.49 | 50 | (Paciga et al., 2016) |
| Paris (winter) | 0.3 | 0.29 | 0.41 |  | 50 | (Paciga et al., 2016) |
| Dongying (spring) | 0.52 | 0.26 | 0.22 | 0.85 | 20.2 | This study |
| **Biogenic** | **ELVOCs** | **LVOCs** | **S/IVOCs** | **O:C** | **RT(s)** | **References** |
| United State (summer) | 0.41 | 0.43 | 0.16 | 0.98 | 10-15 | (Hu et al., 2016b) |
| Amazon | 0.52 | 0.37 | 0.11 |  |  | (Hu et al., 2016b) |

**Table S3. Summary of fractions of ELVOCs, LVOCs and S/IVOCs of FFOA, the residence time (RT) of TD as well as the O:C of aerosols.**

| Ambient | ELVOCs | LVOCs | S/IVOCs | O:C | RT(s) | References |
|---|---|---|---|---|---|---|
| Beijing HOA (summer) | 0.14 | 0.11 | 0.75 | 0.17 | 7.4 | (Xu et al., 2021) |
| Beijing FFOA (winter) | 0.05 | 0.25 | 0.7 | 0.1 | 10 | (Xu et al., 2021) |
| Gucheng HOA (winter) | 0.09 | 0.23 | 0.68 | 0.12 | 10 | (Xu et al., 2021) |
| Gucheng CCOA (winter) | 0.1 | 0.28 | 0.62 | 0.18 | 10 | (Xu et al., 2021) |
| Mexico City (spring) | 0.13 | 0.27 | 0.6 | 0.2 | 21.2 | (Xu et al., 2021) |
| Paris (winter) | 0.11 | 0.29 | 0.6 | 0.1 | 50 | (Paciga et al., 2016) |
| Paris (summer) | 0.13 | 0.24 | 0.63 | 0.21 | 50 | (Paciga et al., 2016) |
| Athens (winter) | 0.3 | 0.42 | 0.28 | 0.1 | 28 | (Louvaris et al., 2017) |
| Dongying (spring) | 0.44 | 0.2 | 0.37 | 0.55 | 20.2 | This study |
| **Laboratory** | **ELVOCs** | **LVOCs** | **S/IVOCs** | **O:C** | **RT(s)** | **References** |
| Diesel POA | 0 | 0.03 | 0.97 |  | 56 | (May et al., 2013a) |
| Diesel | 0 | 0.02 | 0.98 |  | 16 | (Grieshop et al., 2009b) |
| Diesel | 0 | 0.09 | 0.91 |  | 16 | (Grieshop et al., 2009a) |
| Traffic tunnel POA | 0 | 0.12 | 0.88 |  | 10.6 | (Li et al., 2016) |
| Gasoline POA | 0 | 0.27 | 0.73 |  | 56 | (May et al., 2013b) |

**Table S4. Summary of fractions of ELVOCs, LVOCs and S/IVOCs of BBOA, the residence time (RT) of TD as well as the O:C of aerosols.**

| Ambient | ELVOCs | LVOCs | S/IVOCs | O:C | RT(s) | References |
|---|---|---|---|---|---|---|
| Gucheng (winter) | 0 | 0.48 | 0.52 | 0.21 | 10 | (Xu et al., 2021) |
| Mexico City (spring) | 0.04 | 0.27 | 0.69 | 0.38 | 21.2 | (Cappa and Jimenez, 2010) |
| Athens (winter) | 0.09 | 0.39 | 0.52 | 0.27 | 28 | (Louvaris et al., 2017) |
| Dongying (spring) | 0.51 | 0.38 | 0.11 | 0.37 | 20.2 | (Sato et al., 2018) |
| Paris (winter) | 0.19 | 0.3 | 0.51 | 0.1 | 50 | (Paciga et al., 2016) |
| Laboratory | ELVOCs | LVOCs | S/IVOCs | O:C | RT(s) | References |
| Wood smoke | 0 | 0.05 | 0.95 |  | 16 | (Grieshop et al., 2009b) |
| Wood smoke | 0 | 0 | 1 |  | 16 | (Grieshop et al., 2009a) |
| BBOA | 0 | 0.2 | 0.8 |  | 56 | (May et al., 2013c) |

**Table S5. Summary of fractions of ELVOCs, LVOCs and S/IVOCs of OOA, the residence time (RT) of TD as well as the O:C of aerosols.**

| Anthropogenic | ELVOCs | LVOCs | S/IVOCs | O:C | RT(s) | References |
|---|---|---|---|---|---|---|
| Ambient | | | | | | |
| Beijing OPOA (winter) | 0 | 0.32 | 0.68 | 0.34 | 10 | (Xu et al., 2021) |
| Gucheng SOA (winter) | 0 | 0.31 | 0.69 | 0.63 | 10 | (Xu et al., 2021) |
| Beijing LO-OOA (winter) | 0 | 0.36 | 0.64 | 0.68 | 10 | (Xu et al., 2021) |
| Beijing LO-OOA (summer) | 0 | 0.27 | 0.73 | 0.76 | 7.4 | (Xu et al., 2021) |
| Beijing MO-OOA (winter) | 0 | 0.4 | 0.6 | 0.86 | 10 | (Xu et al., 2021) |
| Beijing MO-OOA (summer) | 0 | 0.38 | 0.62 | 1.3 | 7.4 | (Xu et al., 2021) |
| Mexico City SV-OOA (spring) | 0.16 | 0.40 | 0.43 | 0.66 | 21.2 | (Cappa and Jimenez, 2010) |
| Paris OOA (summer) | 0.3 | 0.25 | 0.45 | | 50 | (Paciga et al., 2016) |
| Paris OOA (winter) | 0.3 | 0.25 | 0.45 | 1.12 | 50 | (Paciga et al., 2016) |
| Athens OOA (winter) | 0.42 | 0.29 | 0.29 | 0.5 | 28 | (Louvaris et al., 2017) |
| Transported-OOA (spring) | 0.69 | 0.19 | 0.12 | 1.02 | 20.2 | This study |
| Background-OOA (spring) | 0.56 | 0.22 | 0.22 | 1.1 | 20.2 | This study |
| Mexico City LV-OOA (spring) | 0.34 | 0.37 | 0.29 | 0.77 | 21.2 | (Cappa and Jimenez, 2010) |
| Laboratory | | | | | | |
| 1,3,5-TMB+OH dry | 0.01 | 0.1 | 0.88 | | 13 | (Sato et al., 2019) |
| 1,3,5-TMB+OH dry (aging) | 0.04 | 0.2 | 0.76 | | 13 | (Sato et al., 2019) |
| pentadecane-SOA | 0.04 | 0.54 | 0.42 | 0.53 | 15 | (Faulhaber et al., 2009) |
| Biogenic | ELVOCs | LVOCs | S/IVOCs | O:C | RT(s) | References |
| Ambient | | | | | | |
| IEPOX-SOA US | 0.6 | 0.37 | 0.03 | 0.51 | 10-15 | |
| IEPOX-SOA Amazon | 0.54 | 0.44 | 0.02 | 0.74 | 10-15 | |
| Laboratory | | | | | | |
| a-Pinene Ozonolysis | 0.005 | 0.14 | 0.85 | | 13 | (Sato et al., 2018) |
| a-Pinene Ozonolysis (dry) | 0.005 | 0.18 | 0.82 | | 13 | (Sato et al., 2018) |

|  |  |  |  |  |
|---|---|---|---|---|
| a-pinene (low OHexp) | 0.21 | 0.72 | 0.09 | (Ylisirniö et al., 2020) |

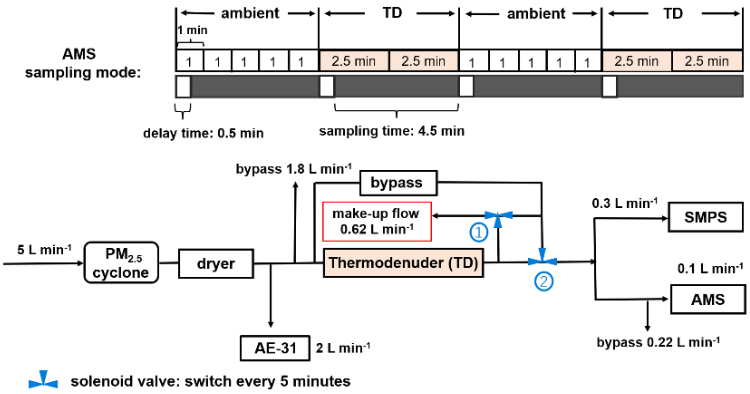

**Figure S1.** Brief schematic plot of sampling line in this campaign. The two solenoid valves control the switch of AMS and SMPS sampling lines to be ambient or TD lines. No matter whether ambient or TD lines were sampled by the SMPS and AMS, there is always a make-up flow to sample the other line for refreshing the air in the pipes.

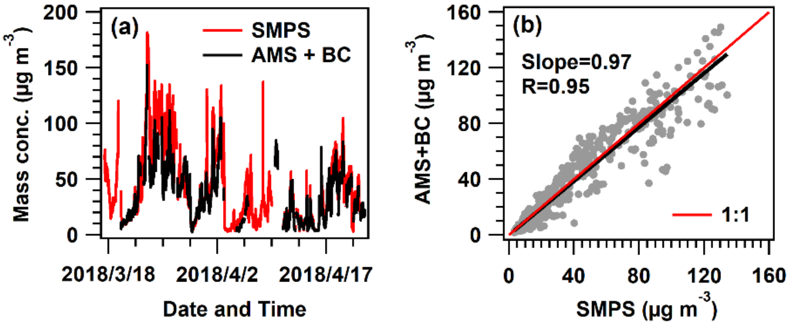

**Figure S2.** (a) Time series of total mass concentration of AMS (including equivalent BC from AE31) and SMPS in this campaign; (b) The scatter plot of calculated mass concentrations from AMS vs. mass from SMPS.

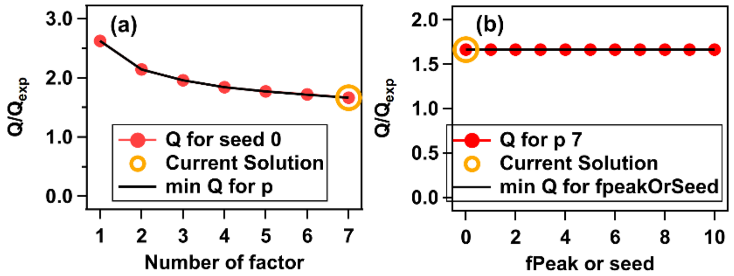

**Figure S3.** Values of (a) $Q/Q_{exp}$ of different solutions and (b) fpeaks or seeds for free PMF.

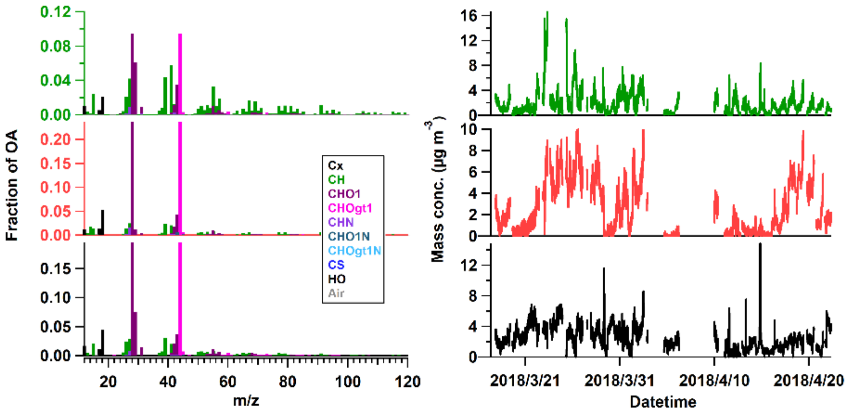

**Figure S4.** 3-factor solution of free PMF results.

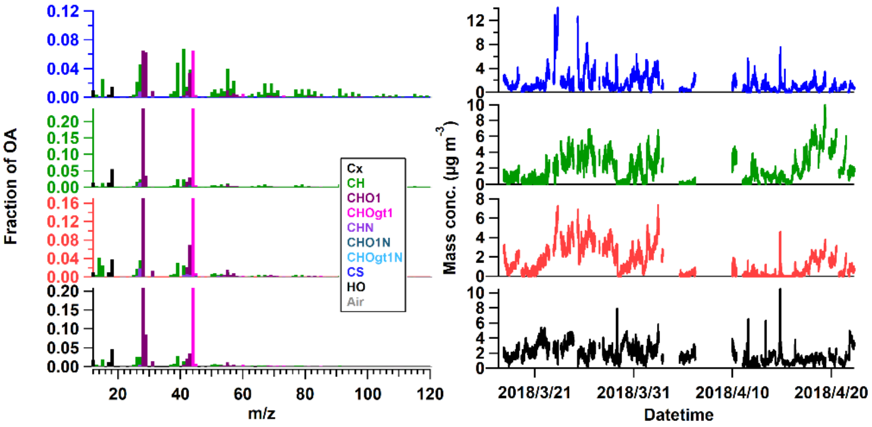

**Figure S5. 4-factor solution of free PMF results.**

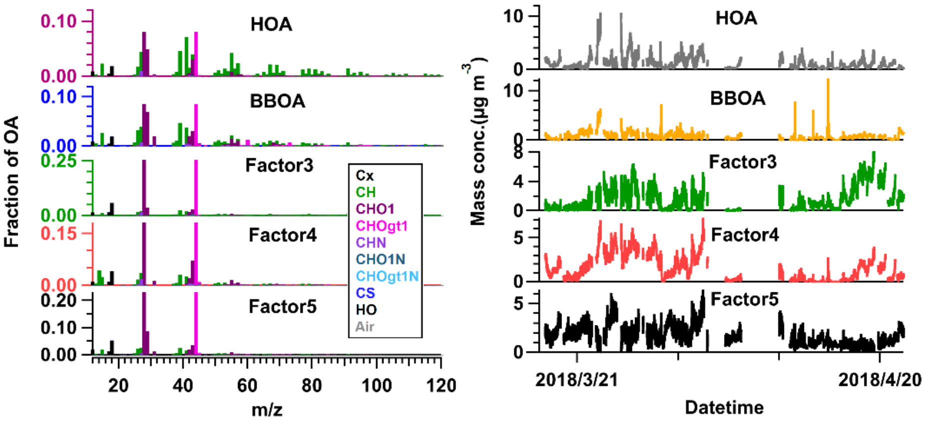

**Figure S6. 5-factor solution of free PMF results. Splitting OOA factors were found for Factors 3-5.**

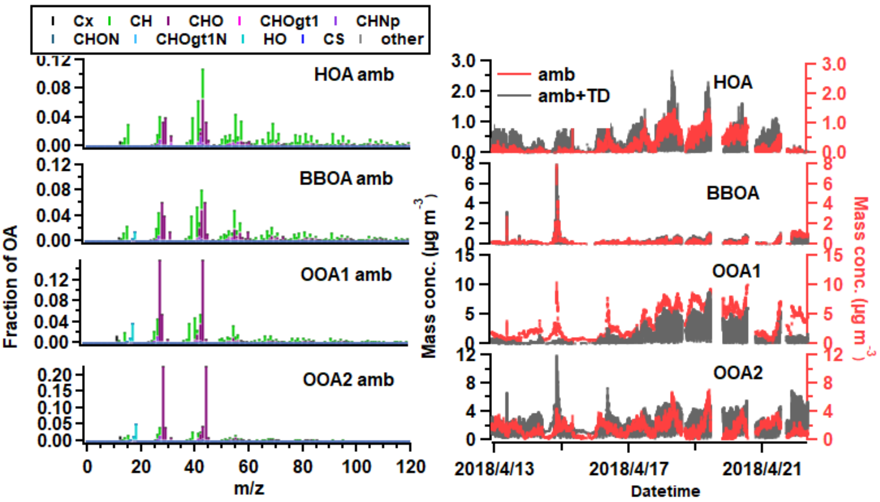

**Figure S7. Comparison of OA factors variations between ambient (red) and ambient + TD (grey) resolved by ME-2 when constraining both HOA and BBOA factors. The solution of four factors were shown here.**

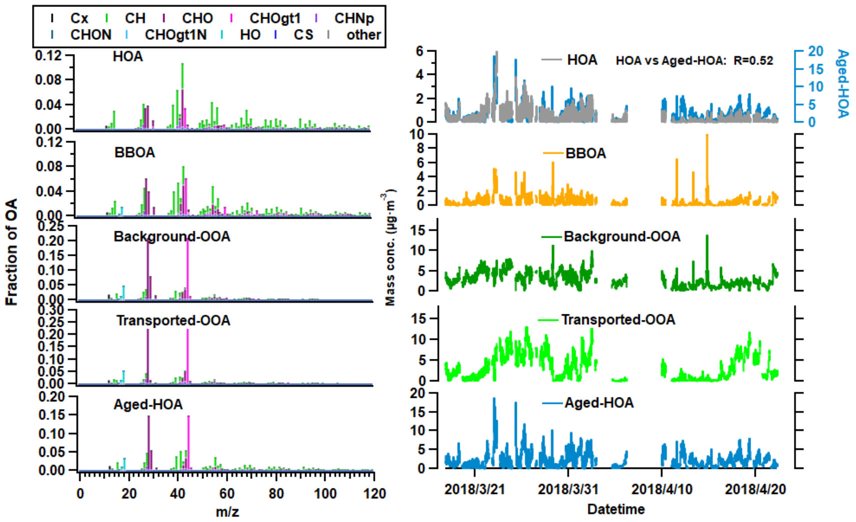

Figure S8. Spectra and time series of 5 factors when constraining both HOA and BBOA. The constrained-HOA show a good correlation with aged-HOA.

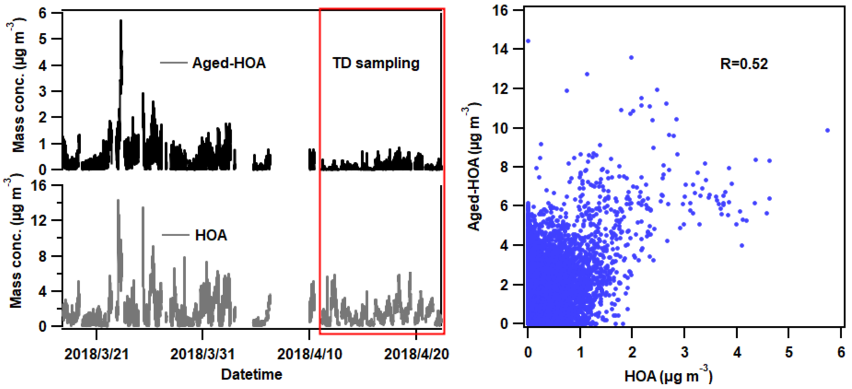

Figure S9. Comparison of time series between constrained HOA and aged-HOA of 5-factor solution when constraining both HOA and BBOA in ME-2.

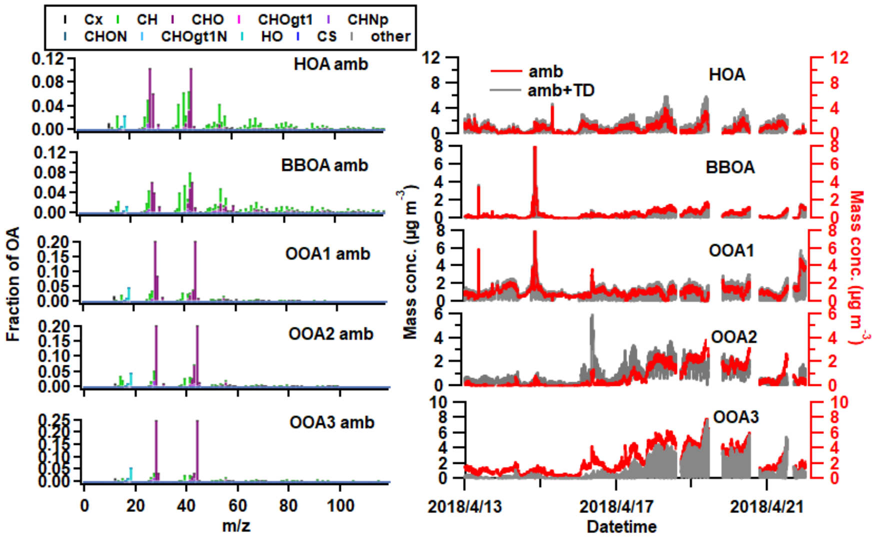

Figure S10. The 5-factor solution when only BBOA was constrained in ME-2.

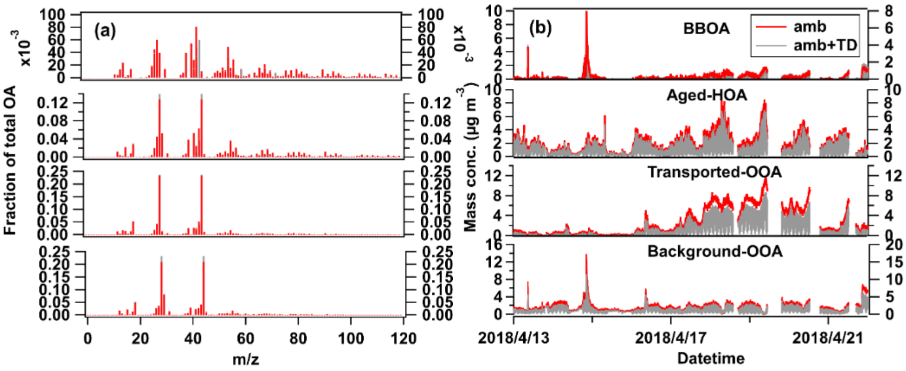

**Figure S11. Comparison of OA factors and spectra between ambient (red) and ambient + TD (grey) resolved by ME-2 when only constraining BBOA.**

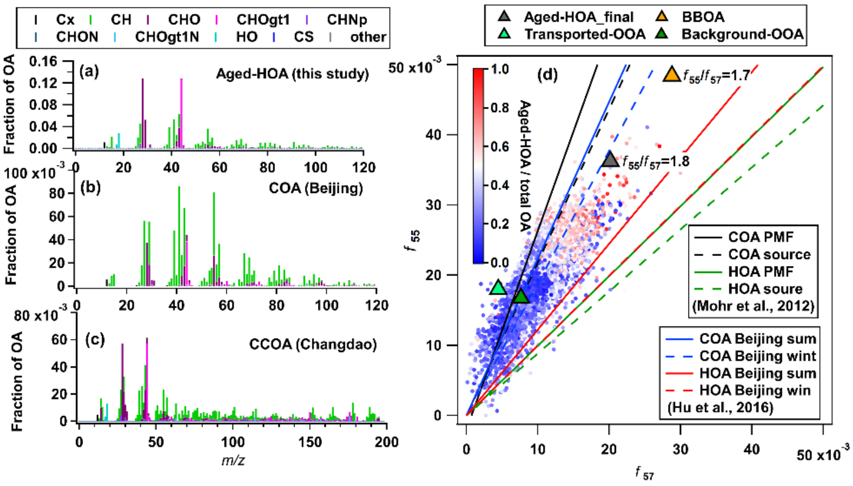

**Figure S12. Spectra of (a) aged-HOA in this study; (b) COA in Beijing; (c) CCOA in Changdao; (d) Scatterplots between $f_{55}$ versus $f_{57}$ in this study. The lines in panel (d) are the range of different sources reported by Mohr et al. (2012) and Hu et al. (2016a).**

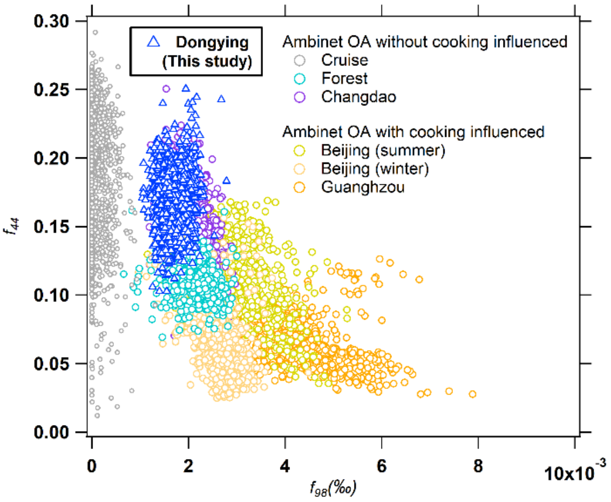

**Figure S13. Scatterplots of $f_{44}$ vs. $f_{98}$, from different studies, including observation sites with/without cooking influenced.**

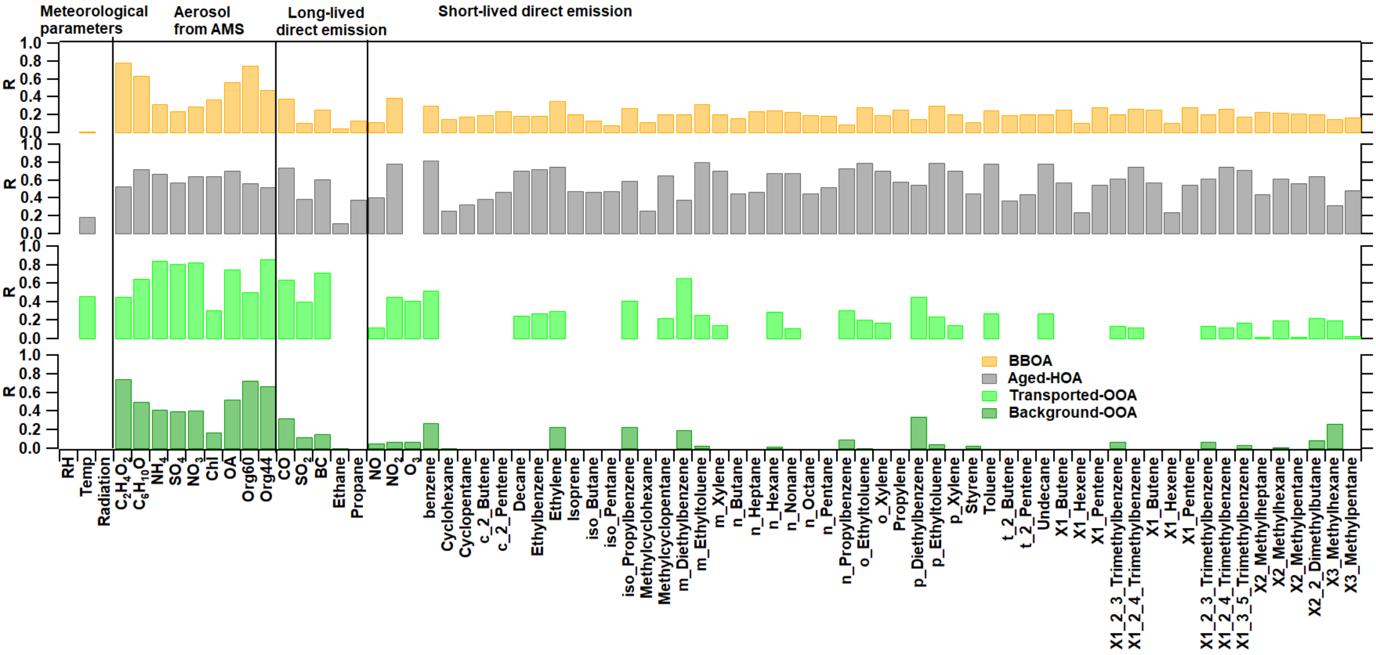

Figure S14. Pearson correlation coefficients for BBOA, aged-HOA, transported-OOA and background-OOA versus species listed in x-axis. Negative values are not shown here.

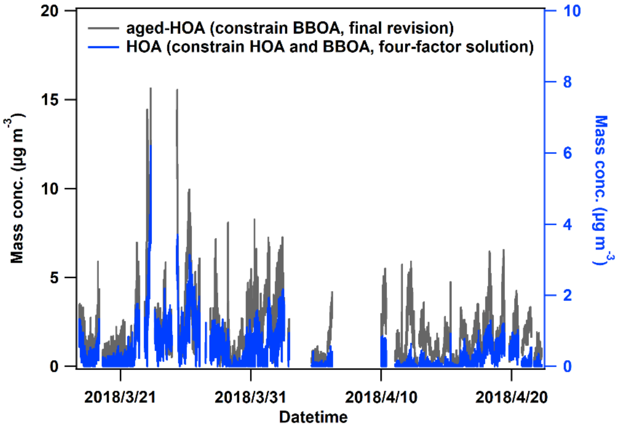

Figure S15. Time series of aged-HOA and POA that resolved when constrained standard HOA spectrum.

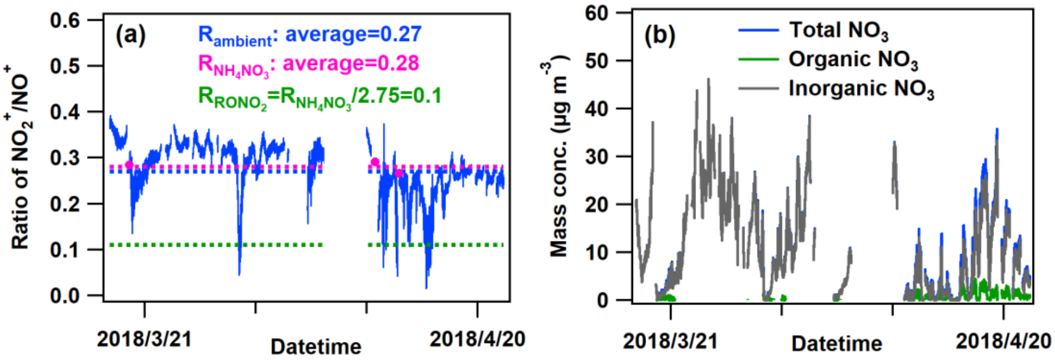

Figure S16. (a) Time series of the ratio of $NO_2^+/NO^+$ for ambient nitrate ($R_{ambient}$), pure ammonium nitrate ($R_{NH4NO3}$) and organic nitrate particles ($RONO_2$); (b) Time series of organic and inorganic nitrate based on the ratios of $NO_2^+/NO^+$ (Farmer et al., 2010; Day et al., 2021).

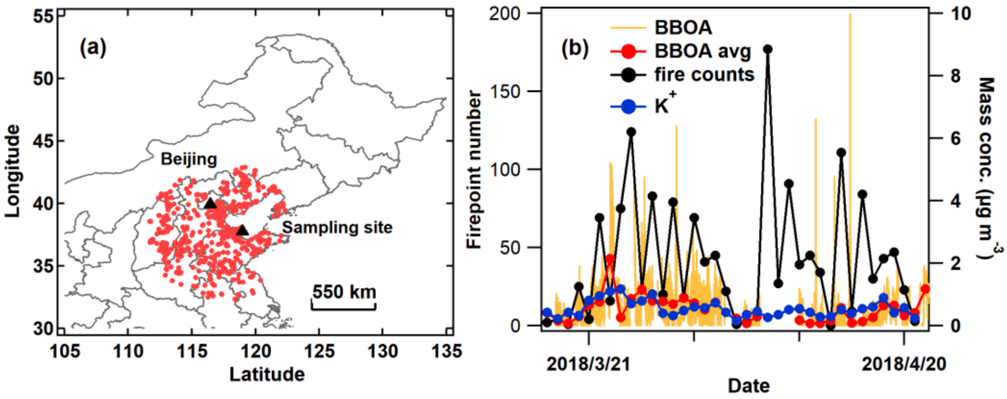

**Figure S17.** (a) Map of fire points in NCP during polluted period obtained by the Fire Information for Resource Management System (FIRMS) (https://firms.modaps.eosdis.nasa.gov/map); (b) Time series of fire points (left axis), mass concentrations of BBOA (per second and per day) and $K^+$.

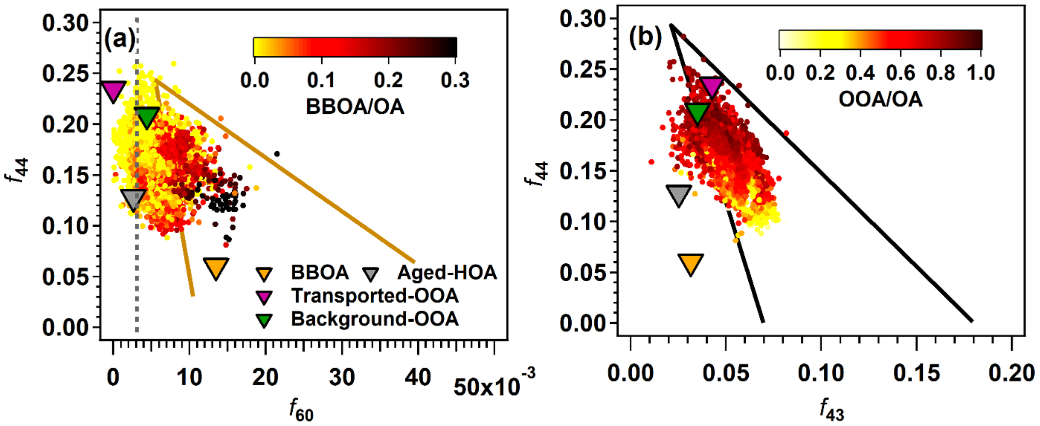

**Figure S18.** Scatter plots of (a) $f_{44}$ vs. $f_{60}$ and (b) $f_{44}$ vs. $f_{43}$, color-coded by the fraction of BBOA and OOA respectively. According to Cubison et al. (2011), the brown triangle (a) is the biomass burning-influence area and the grey dashed line is the background value of $f_{60}$ (=0.003) in non-biomass burning influenced areas. The black triangle in (b) represents OA oxidation area developed by .

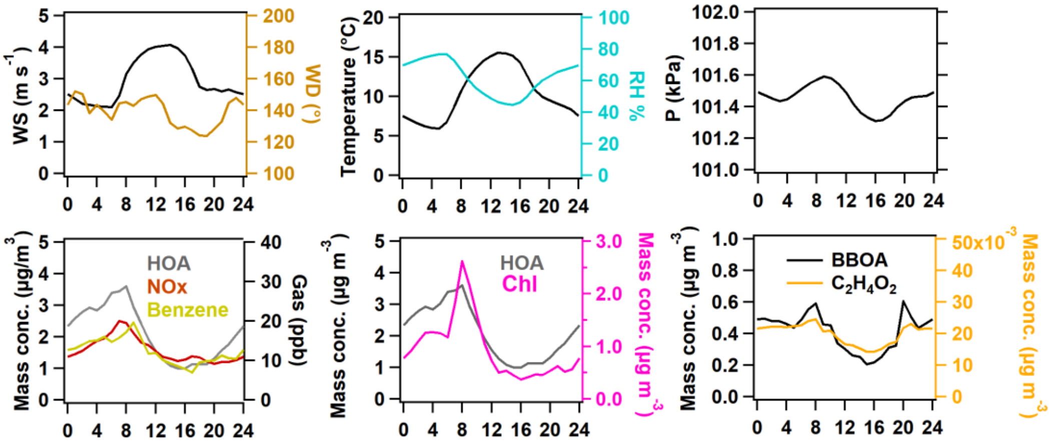

**Figure S19.** Average diurnal variations of meteorological parameters, OA factors and tracers in the entire study.

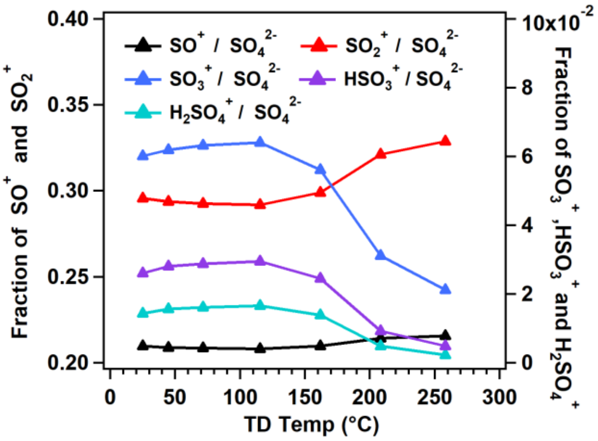

**Figure S20. Variations in ratios of $SO^+/SO_4^{2-}$, $SO_2^+/SO_4^{2-}$, $SO_3^+/SO_4^{2-}$, $HSO_3^+/SO_4^{2-}$, $H_2SO_4^+/SO_4^{2-}$.**

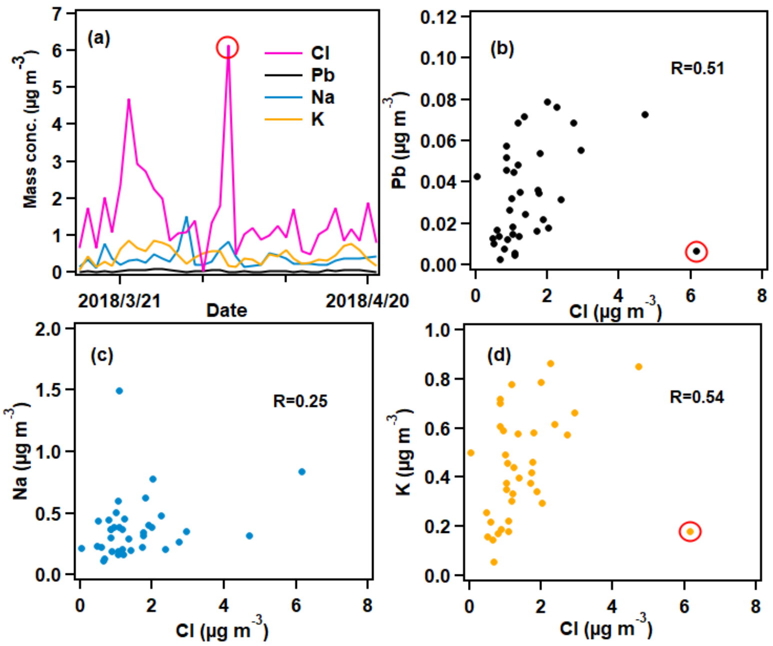

**Figure S21. Time series $Na^+$, $K^+$, $Pb^+$, and $Cl^-$ of measured by offline line technique, as well as the scatterplots between anions and cations. The discrete points surrounded by red circles are not used when calculating Pearson correlation coefficients.**

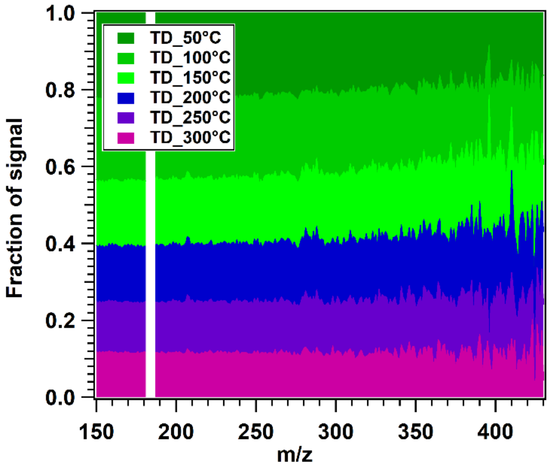

**Figure S22. The fraction of ions (m/z 150-300) detected by AMS (unit mass resolution, V mode) at different TD temperatures.**